HAL
open science

Structural properties and Raman spectra of columbite-type NiNb2–V O6 synthesized under high pressure

J.P. Pena, Pierre Bouvier, O. Isnard

To cite this version:

J.P. Pena, Pierre Bouvier, O. Isnard. Structural properties and Raman spectra of columbite-type NiNb2–V O6 synthesized under high pressure. Journal of Solid State Chemistry, 2020, 291, pp.121607. 10.1016/j.jssc.2020.121607 . hal-02921507

HAL Id: hal-02921507

https://hal.science/hal-02921507v1

Submitted on 18 Nov 2020

HAL is a multi-disciplinary open access archive for the deposit and dissemination of scientific research documents, whether they are published or not. The documents may come from teaching and research institutions in France or abroad, or from public or private research centers.

L'archive ouverte pluridisciplinaire **HAL**, est destinée au dépôt et à la diffusion de documents scientifiques de niveau recherche, publiés ou non, émanant des établissements d'enseignement et de recherche français ou étrangers, des laboratoires publics ou privés.

Structural properties and Raman spectra of columbite-type $NiNb_{2-x}V_xO_6$ synthesized under high pressure

J. Peña[1,2], P. Bouvier[1], O. Isnard[1]

April 24, 2020

[1]Université Grenoble Alpes, Institut Néel CNRS, 25 rue des Martyrs, 38042, Grenoble, France
[2]Instituto de Física, Universidade Federal do Rio Grande do Sul, Av Bento Gonçalves 9500, 91501-970 Porto Alegre, Brazil

Abstract

The complete set of structural parameters of the new series of compounds $NiNb_{2-x}V_xO_6$ ($0 \leq x \leq 2$) with the columbite-type structure is presented here. In the samples containing vanadium, this crystalline structure was stabilized by synthesis in conditions of high pressure and high temperature. The evolution of the vibrational Raman spectrum produced when the vanadium is substituted for niobium along the series is also presented and discussed. This evolution is interpreted by taking into account the changes in the local structural environment of the niobium/vanadium atoms and its influence over the nickel-oxygen bonds around them. The presence of vanadium atoms favors an increasing of the symmetry in the arrangement of oxygen atoms around the nickel-ones; in counterpart the vanadium is in an octahedral environment which is more distorted than that of the niobium. Because of these apparently subtle differences, the homogeneous percolation of vanadium in the solid solution $NiNb_{2-x}V_xO_6$ is not possible.

1 Introduction

The family of oxides with formula AB_2O_6 is formed by a set of compounds with such a rich variety of physical properties and crystalline structures, that the only characteristic that remains constant among them is the stoichiometry proportion 1:2:6 for the atoms "A", "B" and "O", respectively. In this formula, "A" represents a divalent cation of some alkaline-earth or transition metal, "B" represents a pentavalent transition metal of the fifth group, and "O" represents oxygen. The physical properties are ruled by both the cations A and B[1], but the crystalline structure is in most cases defined by the atom in the B position. Because of it, the subfamilies of AB_2O_6 compounds

[1]In this text, B-atom or B-cation always refers to the atom occupying the "B" position in the general formula AB_2O_6 and not to the chemical element boron.

are commonly classified as Vanadates, Niobates, or Tantalates, depending if the B position is occupied by vanadium, niobium or tantalum, respectively. In general terms, when synthesized at room pressure, the symmetry of the crystalline lattice reduces from tetragonal in the Tantalates to orthorhombic in the Niobates to even triclinic in the Vanadates. Here we will use the Niobate $NiNb_2O_6$ which stabilizes in a columbite type structure (group 60, *Pbcn*) as reference and starting compound for the synthesis of our series of $NiNb_{2-x}V_xO_6$ samples.

In the structure of $NiNb_2O_6$ both Ni^{+2} and Nb^{+5} cations are surrounded by six oxygen atoms forming an octahedral environment around them. The octahedra around the Ni-atoms are slightly distorted, but those around the Nb-ones are so distorted that they are sometimes called "cuboids". In the unitary cell of the $NiNb_2O_6$ the lattice parameters satisfy the relation $a > b > c$. This cell is formed by layers of Ni and Nb octahedra stacked along the $a-$axis forming an alternated sequence Ni–Nb–Nb–Ni–Nb–Nb–Ni [1]. Along the c-axis both the octahedra around the Ni and Nb cations form zigzag edge-sharing chains. On the ab-plane the Ni^{+2} chains are arranged in an isosceles triangular geometry [2, 3] which confers a magnetic behavior of low-dimensional character [3] which is one of the most interesting properties of this compound. Another recently discovered property of the $NiNb_2O_6$ is its potential as a photocatalyst under visible light irradiation for the efficient production of H_2 from water splitting [4].

The group of the AB_2O_6 Vanadates is the richest one in terms of polymorphism. For example, the compounds AV_2O_6 present a monoclinic structure of space group *C2/m* when A = Mn, Cd, Mg, or Zn [5, 6]; meanwhile, depending on the temperature of synthesis, at room pressure the structure of CoV_2O_6 can be monoclinic ($\alpha-$phase) or triclinic ($\gamma-$phase) [7, 8, 9], and it is unequivocally triclinic when A = Ni, Cu. The Vanadates with A = Ni, Mg, Co, Zn, Mn and Cd were produced in the columbite-type structure in 1973 by using conditions of synthesis of high pressure/high temperature (HPHT) [10]; at the time only partial studies on the structure were done. Recently, new and more powerful experimental techniques make possible the study of the physical properties of these compounds thus renewing the interest on them. In 2017 the structural and magnetic properties of the *Pbcn*-MnV_2O_6 [11] were first reported, and it was later found that the magnetic order is suppressed in the *Pbcn*-$MnNbVO_6$ [5]. A study of the Raman-spectrum at different values of externally applied pressure on *Pbcn*-MgV_2O_6 was also recently reported in Ref. [12]. To our best knowledge no other experimental studies in Vanadates with the columbite structure, which is rather unusual for these compounds, were reported. Here we deeply explore both the structure and vibrational Raman spectrum of the whole series of samples $NiNb_{2-x}V_xO_6$, all of them crystallized in the *Pbcn* space group.

Among the Vanadates we will use as reference compound the NiV_2O_6 which at room pressure crystallizes in the $P\bar{1}$ space group. This structure is formed by edge-connected NiO_6-octahedra forming 1D chains along the c-axis [13]. Those chains are separated from each other by two planes of alternated octahedral and tetrahedral arranges of oxygen atoms around the V^{+5} ions [13]. The $P\bar{1}$-NiV_2O_6 presents an antiferromagneticaly ordered phase below $T_N = 16.4$ K, and recent studies have proved it as a visible-light-active photoanode for photoelectrochemical (PEC) water oxidation [14].

In general, the vanadium oxides have a large range of applications coming from the different

Table 1: Synthesis parameters to obtain samples of $NiNb_{2-x}V_xO_6$ ($0 < x \leq 2$) in the *Pbcn* phase.

Compound	P (GPa)	T (℃)	time at max P and T (min)
$NiNb_{2-x}V_xO_6$, $1 \leq x \leq 2$	5.9	900	60
$NiNb_{2-x}V_xO_6$, $x = 0.66$	5.9	1100	20

physical properties that are observed in these compounds. Among the enumerated as the most recent applications discovered of vanadium oxides cited in the reference review by Shvets. *et. al.* [15] are cathode materials for batteries, electro-chromatic systems, supercapacitors, smart windows, optical switching devices and memory elements. The diversity of physical properties observed in the Vanadates is a consequence of the several types of bonds that the different valence states of the vanadium make possible. In this respect, the sensitivity to the local atomic arrangement of Raman spectroscopy make it a specially useful technique to understand the physical properties of Vanadates.

2 Experimental section

Samples of $NiNb_{2-x}V_xO_6$ ($0 < x < 2$) were obtained by submitting stoichiometric mixtures of the starting powders $P\bar{1}$-NiV_2O_6 and *Pbcn*-$NiNb_2O_6$ to the extreme conditions of HPHT shown in Table 1. All the synthesis were performed in a CONAC-40 press. The pressure was slowly increased/reduced; the temperature was risen only after the maximal pressure was reached and it was quenched before the pressure started to be reduced. The sample $NiNb_2O_6$, which is also a precursor for other samples, was synthesized by mixing stoichiometric quantities of high purity NiO and Nb_2O_5; this mix was heated at 1300 ℃ for 48 h in a muffle-type oven and then left to cool at the natural cooling rate of the furnace. In order to obtain the NiV_2O_6, a mixture of high purity Ni-acetate ($NiC_4H_{14}O_8$) and V_2O_5 was used. An excess of 7% in mass with respect to the stoichiometrically necessary quantity of V_2O_5 was used in order to avoid the formation of $Ni_2V_2O_7$ which was identified as an spurious phase in previous synthesis. The thermal treatment was performed at 620 ℃ for 48 h. No impurities were observed on the X-rays diffraction pattern for the triclinic $P\bar{1}$-NiV_2O_6. The *Pbcn*-NiV_2O_6 ($x = 2$) was obtained by submitting the pure powder sample of the triclinic phase to the same conditions showed in Table 1.

X-rays diffraction (XRD) patterns of finely ground powder samples were acquired in a Bruker D8 Endeavor diffractometer with copper anode ($\lambda_\alpha = 1.5418$ Å). All the measurements were carried out at room temperature in the Bragg-Brentano geometry. The diffraction patterns were refined with the Rietveld method by considering pseudo-Voigt shaped peaks. The software used for the whole refinement process was FULLPROF [16]. Some of the figures showing the crystalline structure were elaborated by using VESTA [17].

The micro-Raman measurements were carried out at room temperature and pressure by using a custom-built spectrometer with monochromator ACTON Spectra Pro 2750. This device is equipped with a 1800 mm^{-1} grating blazed at 500 nm and a Pylon eXcelon CCD camera; a set of three Bragg

filters BNF-Optigrate was used in order to reject the excitation of the 514.4 nm (Cobolt Fandango) laser. The spectra were recorded in backscattering geometry with a 40x objective used both to focus the incident laser beam and to collect the scattered light. The spectrometer was calibrated in wavenumber by using the lines 540.056, 585.249, 588.190, 594.483 and 597.553 nm of the Princeton-Instrument Ne-Ar lamp.

The Raman signal of the samples with $0.5 < x \leq 2$ is rather weak; however, as those samples are relatively dark, the laser power was set low enough ($W \sim 0.6$ mW) to avoid any influence of laser heating on the Raman spectra. After the optimization of the beam power, the data were acquired by taking the mean of two frames of 240 s each. In the case of the $NiNb_2O_6$ (yellow powder) the Raman signal is very intense; thus, in order to avoid saturating the detector, the mean to obtain the final spectrum was taken over ten frames of only 10 s each. The Raman spectra were decomposed with Lorentzian functions using Fityk software (version 1.3.1) [18].

3 Results and discussion

3.1 X-rays diffraction measurements

An investigation of the XRD patterns reveals that the structure of all the synthesized samples of $NiNb_{2-x}V_xO_6$ retain the orthorhombic symmetry described by the *Pbcn*-space group. The lattice parameters of the *Pbcn*-$NiNb_{2-x}V_xO_6$ system shrink when the quantity of vanadium increases as shown in Fig. 1. This effect follows the Vegard's law, and it is expected from the smaller ionic radius of the pentavalent vanadium ions with respect to the niobium ones. Between the samples $x = 0$ and $x = 2$ the parameters a, b and c were noticeably reduced by 4.8%, 2.7%, and 4.1%, respectively. These values are almost the same that those found in Ref. [5] for A = Mn, and point to a remarkable anisotropic response of the atomic arrangement to chemical substitution of the B-site in both systems. This response seems to be independent of the magnetic nature of the A-ions interactions.

The complete set of structural parameters for each of the studied samples and the agreement factors of the Rietveld refinements are reported in Table 2. One example of the fitted diffraction pattern is shown in Fig. 2 for the sample $x = 1$. Our results for sample $x = 0$ are in good agreement with those reported in Ref. [3]. For all samples, except for that with $x = 0.66$, the Rietveld refinement was completed by taking into account only the phase with the desired stoichiometry; thus we infer that our samples are formed by one single structural phase crystallizing in the *Pbcn* group. Several attempts were made to obtain one sample with one single phase of $NiNb_{1.5}V_{0.5}O_6$. In all the attempts, it was necessary to include a pure and non-distorted phase of $NiNb_2O_6$ in order to complete the refinement; the best result was obtained when we used the most extreme conditions of pressure and temperature shown on the second row of Table 1. We got one mixed sample, here called $x = 0.66$, where the impurity phase ($NiNb_2O_6$) represents 27% of the total mass of the sample; with this, we calculated that the main phase, more concentrated in V than what was initially intended, corresponds to the chemical formula $NiNb_{1.34}V_{0.66}O_6$. This stoichiometry is in perfect agreement with the composition dependence of the lattice parameters plotted in Fig. 1. The difficulty of obtaining a pure sample of $NiNb_{1.5}V_{0.5}O_6$ reflects the stability of the orthorhombic structure of

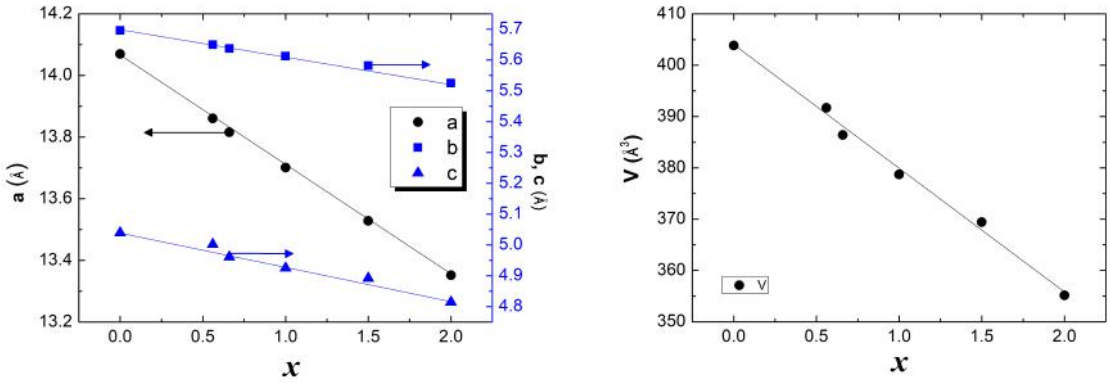

Figure 1: Variation of the structural parameters (left) and the volume of the orthorhombic cell (right) with increasing vanadium content in $NiNb_{2-x}V_xO_6$. Solid lines are guides to the eyes.

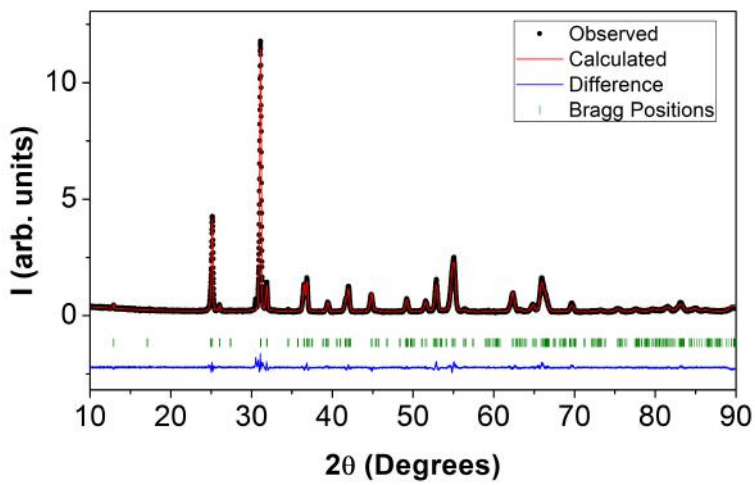

Figure 2: Result of the Rietveld refinement performed at room temperature on the XRD pattern measured for the sample $NiNbVO_6$. The green marks indicate the positions of the expected Bragg peaks from the Pbcn structure

Table 2: Cell parameters and atomic positions of the $NiNb_{2-x}V_xO_6$ (*Pbcn*-space group) studied samples as derived from Rietveld refinements of XRD patterns at room temperature

$x =$		0	0.66	1	1.5	2
Ni	x	0	0	0	0	0
	y	0.1612(7)	0.1613(9)	0.1646(6)	0.166(1)	0.1565(4)
	z	0.25	0.25	0.25	0.25	0.25
Nb/V	x	0.1601(1)	0.1619(2)	0.1628(1)	0.16477(3)	0.1645(2)
	y	0.3194(2)	0.3222(3)	0.3225(3)	0.3252(5)	0.3242(3)
	z	0.7502(9)	0.753(1)	0.751(2)	0.749(1)	0.745(1)
O1	x	0.0843(6)	0.0852(5)	0.0949(3)	0.1010(6)	0.0939(5)
	y	0.383(1)	0.372(1)	0.395(1)	0.389(2)	0.412(1)
	z	0.416(2)	0.419(2)	0.436(1)	0.458(2)	0.424(2)
O2	x	0.0775(5)	0.083(3)	0.0805(5)	0.0815(8)	0.0882(6)
	y	0.102(1)	0.123(3)	0.126(1)	0.127(3)	0.131(1)
	z	0.919(2)	0.917(3)	0.908(2)	0.903(2)	0.902(2)
O3	x	0.2628(9)	0.261(3)	0.2542(6)	0.251(1)	0.2552(8)
	y	0.125(1)	0.113(3)	0.132(1)	0.131(3)	0.127(2)
	z	0.582(2)	0.584(3)	0.584(2)	0.583(2)	0.602(2)
a (Å)		14.0229(2)	13.8158(4)	13.7013(3)	13.5013(4)	13.3518(2)
b (Å)		5.6769(1)	5.6375(2)	5.6121(1)	5.5649(2)	5.5252(1)
c (Å)		5.0184(1)	4.9611(1)	4.9253(1)	4.8639(1)	4.8145(1)
V (Å^3)		399.51(1)	386.40(2)	378.72(1)	365.44(2)	355.166(8)
R_P (%)		9.07	7.16	6.72	7.13	9.71
R_{WB} (%)		11.5	9.24	9.30	9.77	12.4

the precursor $NiNb_2O_6$ which had already been pointed out in Ref. [19] for the $CaNb_2O_6$. Such stability makes it very difficult to distort the NbO_6 octahedra with only a modest quantity of vanadium atoms, even under conditions of high temperature and pressure.

The octahedral environment of the Ni-atoms in the columbite structure, and the edge-sharing zigzag chains of Ni-octahedra along the $c-$axis are represented in Fig. 3; there, the distances between the central Ni-atom and each of its six nearest neighbor oxygen atoms are defined. These parameters and the distance Ni-Ni along the zigzag chains ($d_{(\text{Ni-Ni})c}$) are reported in Table 3. It is interesting to note here that the three Ni-O interatomic distances, *d1*, *d2*, and *d3*, increase with increasing vanadium content whereas the Ni-Ni distance $d_{(\text{Ni-Ni})c}$, the cell volume and the unitary cell parameters decrease. The angle between each of the oxygen atoms on the shared edge and the corresponding adjacent Ni-atoms along the chain (θ) is also represented in Fig. 3, and its value reported in the last column of Table 3. By looking at the whole set of data contained in Table 3 one can conclude that the characteristic Ni-chains of the columbite structure suffer considerable alterations when the vanadium is substituted for niobium. Specifically, when the

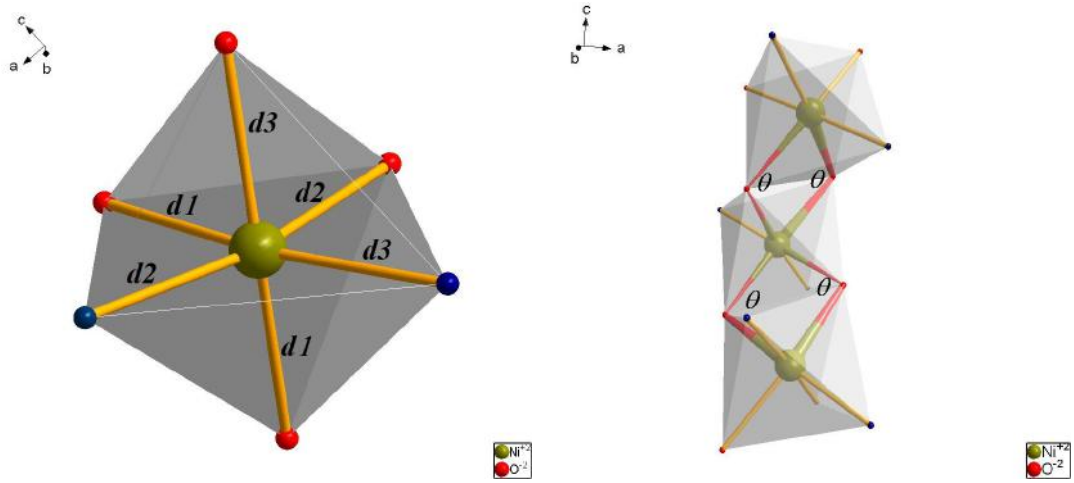

Figure 3: Octahedral environment of the Ni-atoms in the *Pbcn*-structure (the red and blue spheres represent oxygen-atoms with the non-equivalent crystallographic positions named as O1 and O2, respectively, in Table 2). At right, the edge-sharing zigzag Ni-chains along the $c-$axis. The angle Ni-O-Ni connecting the octahedra along the chain is signaled.

quantity of vanadium increases, the Ni-chains are formed by closer Ni-atoms enclosed in larger oxygen-octahedra connected by righter angles.

As the Ni-atoms, the B-cations (B = Nb, V) also present an octahedral environment in the *Pbcn* structure and form chains along the $c-$axis; these chains are represented in Fig. 4. The interatomic distances characterizing the octahedral environment around the B-cations, and the distance between two successive B-atoms along the chains ($d_{(\text{B-B})c}$)are presented in Table 4. It can be seen that the B-octahedra are distorted in such a way that this time there are no pairs of equal distances as it happens for the Ni-octahedra. Besides, Fig. 4 shows that the two oxygen atoms on the shared edge do not occupy equivalent positions, and so the angles between the two successive B-atoms and the two O-atoms on the shared edge are different. The values of these angles are presented in Table 5.

For the chains of B-octahedra both interatomic distances $d_{(\text{B-B})c}$ and $< d_{\text{B-O}} >$ decrease upon increasing vanadium content. Concerning the B-O interatomic distances, *d1*, *d2* and *d3* exhibit a pronounced decrease whereas *d4* and *d5* distances are much less sensitive and *d6* remains almost constant all along the series. This clearly illustrates the importance of these BO_6 octahedra in the *Pbcn* structure in the context that these reductions can indeed be interpreted as the origin of the reduction of the unit cell with increasing x. It is remarkable also that the angles θ_1 and θ_2 evolve in opposite direction with the increasing of x, i.e. θ_1 increases from about 102° to about 109° when x goes from $x = 0$ to $x = 2$, while θ_2 decreases from about 100° to about 97°. These results indicate that the BO_6 pseudo-octahedra are even more distorted when Nb^{+5} is replaced by V^{+5} in the structure.

Table 3: Interatomic distances in ångström between each Ni-atom and the six nearest neighbor oxygen atoms forming its distorted octahedral environment. The last column shows the value of the angle Ni-O-Ni in degrees along the zigzag chains for each of the samples studied here. The mean value of the interatomic distances Ni-O is represented by the symbol $< d_{\text{Ni-O}} >$; all the other symbols are defined in Fig. 3

x	*d1*	*d2*	*d3*	$< d_{\text{Ni-O}} >$	$d_{(\text{Ni-Ni})c}$	θ
0	2.03(1)	2.02(1)	1.92(1)	1.990(4)	3.106(3)	100.1(4)
0.66	2.139(4)	2.0266(5)	1.871(9)	2.0122(4)	3.076(4)	95.1(2)
1.00	2.10(1)	2.07(1)	2.04(1)	2,073(4)	3.081(4)	95.1(5)
1.50	2.11(1)	2.01(1)	2.10(1)	2,078(4)	3.060(6)	95.6(5)
2	2.110(9)	2.055(9)	2.067(9)	2,077(4)	2.957(3)	90.5(4)

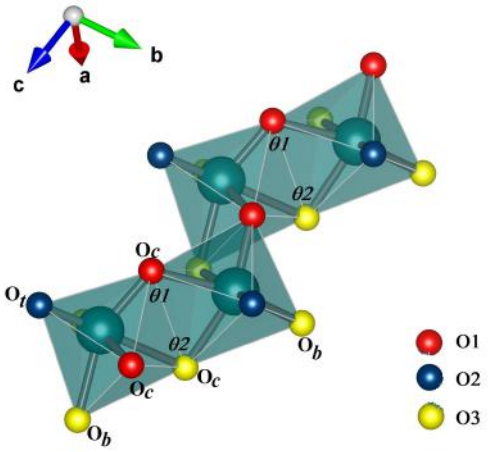

Figure 4: Chain of largely distorted BO_6 octahedra along the $c-$axis in the crystalline structure of the $NiNb_{2-x}V_xO_6$. $O_{t,b,c} \equiv$ oxygen in terminal, bridge, or chain position (see text)

Table 4: Interatomic distances in ångström characterizing the B-octahedra and chains of the $NiNb_{2-x}V_xO_6$ compounds studied here; $< d_{\text{B-O}} >$ is the mean value of the interatomic distances B-O. The subindexes t, b, or c refer to bonds between the central B-atom and an oxygen in the position terminal, bridge, or chain, respectively (see Fig. 4 and text in the Raman spectroscopy section).

x	$d1$-O_b	$d2$-O_t	$d3$-O_c	$d4$-O_c	$d5$-O_b	$d6$-O_c	$< d_{\text{B-O}} >$	$d_{(\text{B-B})c}$
0	2.18(1)	1.89(1)	1.99(1)	2.19(1)	1.99(1)	2.02(1)	2.060(4)	3.241(9)
0.66	2.184(9)	1.760(4)	1.994(3)	2.126(3)	1.98(1)	1.989(6)	2.006(1)	3.189(8)
1.00	2.06(1)	1.74(1)	1.87(1)	2.23(1)	1.85(1)	1.99(2)	1.958(4)	3.167(9)
1.50	2,06(1)	1.75(1)	1.784(5)	2.204(4)	1.71(1)	1.996(6)	1.916(2)	3.112(8)
2	1.942(9)	1.64(1)	1.77(1)	2.10(1)	1.87(1)	2.04(1)	1.897(4)	3.099(8)

Table 5: Angles in degrees between the B and O-atoms connecting the BO_6-octahedra along the $c-$axis in the $NiNb_{2-x}V_xO_6$ compounds. The symbols are represented in Fig. 4

x	$\theta 1$	$\theta 2$
0	101.7(6)	100.2(6)
0.66	99.6(5)	101.6(4)
1.00	108.0(6)	97.2(7)
1.50	111.0(6)	95.5(4)
2	108.6(6)	96.7(5)

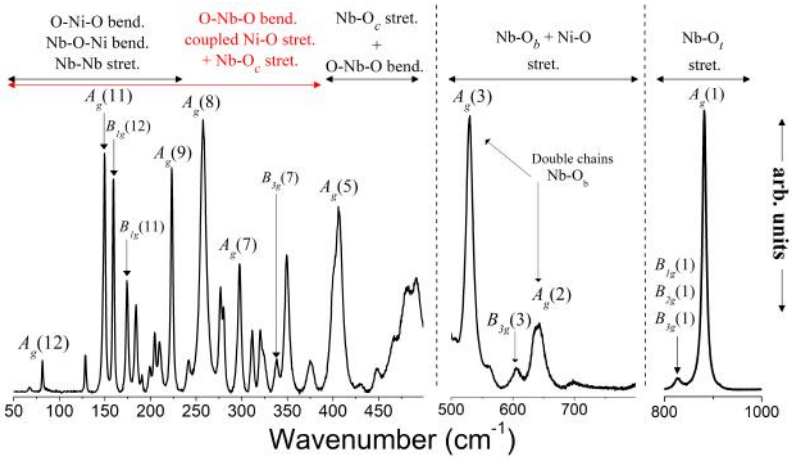

Figure 5: High quality Raman spectrum of the $NiNb_2O_6$. The three regions of relative wavenumber mentioned in the text are separated by the vertical dashed lines. In each region the vertical axis is normalized to the height of the peak with maximum height in each region. Stretching and bending are abbreviated as stret. and bend., respectively.

3.2 Raman spectroscopy

The highly resolved Raman spectrum measured for our sample of $NiNb_2O_6$ ($x = 0$) is shown in Fig. 5; we observed 47 of the 54 expected modes for the structures belonging to the *Pbcn* space group thus providing significant additional information to the previously reported data on this compound. The detailed list of Raman active modes is reported in the supplementary information. The spectrum shown in Fig. 5 is representative of the Raman spectrum of all the Niobates of the AB_2O_6 family. In Refs. [19, 20, 21] Husson *et. al.* made a wide theoretical and experimental study of the Raman and infrared modes of vibration of several Niobates where the position "A" was occupied by Ca, Mg, Mn, Ni, Zn or Cd. The authors established that the Raman spectra of all these Niobates are qualitatively equal at wavenumbers higher than $\bar{\omega} \sim 380$ cm^{-1}. The region in relative wavenumber larger than $\bar{\omega} > 800$ cm^{-1} is dominated by a very intense peak which corresponds to one A_g symmetry mode. This mode is related to the stretching of the Nb-O$_t$ bonds, where O$_t$ denotes the oxygen atoms in the "terminal or free" position which connect the BO_6 octahedra with the adjacent chains of NiO_6 octahedra. Between $\bar{\omega} = 380$ cm^{-1} and $\bar{\omega} = 800$ cm^{-1} the modes correspond to the stretching movements inside the NbO_6 octahedra. There the bonds can imply oxygen atoms in the "bridge" (O$_b$) and "chain" (O$_c$) positions which denote the oxygen atoms connecting two BO_6 octahedra belonging to the same chain, or the oxygen atoms linking two successive BO_6 chains, respectively. Below $\bar{\omega} = 380$ cm^{-1} the peaks observed in the spectrum are due to modes of bending and torsion of the NbO_6 octahedra involving the angles O-Nb-O. In this region, some of those modes are also coupled with displacements of the Ni-atoms. Finally, at very low frequencies ($\bar{\omega} < 100$ cm^{-1}) one observes the modes related to sub-lattices vibrations with respect to each other (for example the harmonic movement of the Ni-atoms with respect to the Nb-ones).

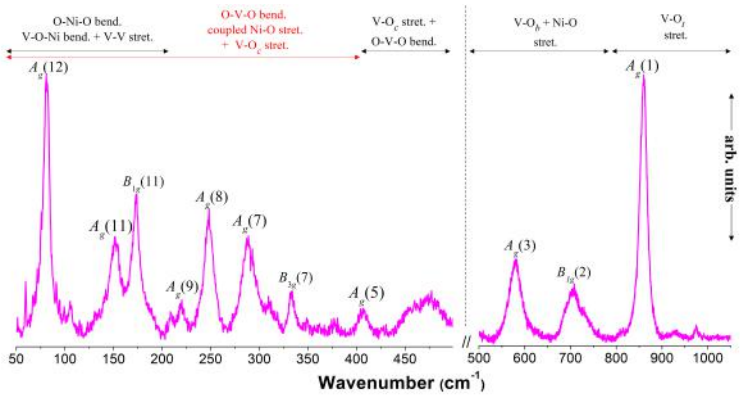

Figure 6: Raman spectrum for the sample NiV_2O_6 with the *Pbcn* structure studied here. The assignement of the modes are presented in Table 6. The vertical axis is normalized to the height of the peak with maximum height in each of the two regions separated by the dashed line. Stretching and bending are abbreviated as stret. and bend., respectively.

The Raman spectrum for sample NiV_2O_6 ($x = 2$) is shown in Fig. 6. To our best knowledge, this is the first reported Raman spectrum of NiV_2O_6 with the unusual columbite-type structure. When compared to each other, the spectrum of sample $x = 2$ presents much wider peaks than that of sample $x = 0$; in the region $\bar{\omega} > 500$ cm^{-1} the FWHM of individual peaks is around 12 cm^{-1} when $x = 0$, while it is around 20 cm^{-1} when $x = 2$. The origin of this widening can reside in the increased structural distortion of the VO_6 octahedra with respect to the NbO_6-ones as already pointed in the previous section. Quantitatively, the calculated distortion [16, 22] ($\Delta = n^{-1}\sum_i^n(\frac{d_i-\bar{d}}{\bar{d}})^2$, where n is the coordination number, and $\bar{d} =< d_{\text{B-O}} >$) of the VO_6 octahedra is $\Delta = 6.7 \times 10^{-3}$, against $\Delta = 2.7 \times 10^{-3}$ for the NbO_6 octahedra. As a consequence of the widening of the Raman peaks for the NiV_2O_6, only a small quantity of modes of vibration could be identified here for that sample. The positions of the peaks that can be identified in the Raman spectra of the two extreme compounds of the series $NiNb_{2-x}V_xO_6$ are presented in the second and nineth columns of Table 6. As none theoretical study on the normal coordinate analysis of the AB_2O_6 compounds with the columbite structure when B = V is available, the identification of the symmetry of the modes presented in the first column of Table 6 was done by comparing our results with those of Raman studies performed in Niobates of the AB_2O_6 family already reported in the literature [20, 21, 23, 24].

Raman spectra acquired for the complete series of $NiNb_{2-x}V_xO_6$ samples at room temperature and pressure are presented together in Fig. 7. It is observed that, as the widening of the Raman peaks seems to be intrinsic to the VO_6 octahedra, this widening is propagated along the samples with intermediate compositions of Nb and V. However, in those samples factors related to the presence of both Nb^{+5} and V^{+5} cations can also contribute to the enlargement of the FWHM. The peaks (or sets of peaks) that seem to be common to the Raman spectrum of most of the samples are signaled by small symbols in Fig. 7. As it will be discussed later, in the samples with $0 < x < 2$ the wide peaks correspond to the sum of several Raman peaks that in most cases can not be separated individually.

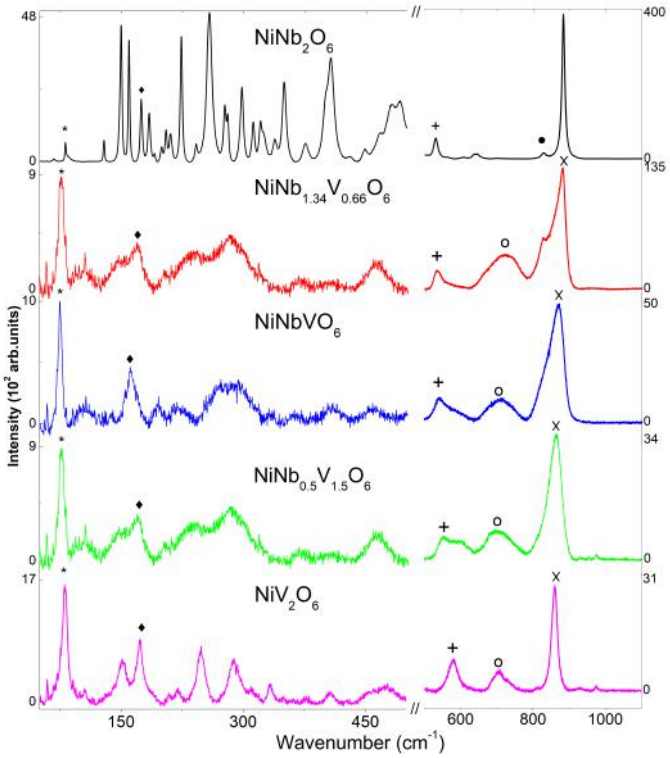

Figure 7: Raman spectra for the complete $NiNb_{2-x}V_xO_6$ series of samples. Some characteristics common to most of the spectra are marked by symbols. Note that the vertical scale is adapted for each sample and wavenumber domain.

Table 6: Raman peaks identified in the spectra of the series $NiNb_{2-x}V_xO_6$ studied here. The relative wavenumber ($\bar{\omega}$) is given in units of cm^{-1}. For samples with $0 < x < 2$ the position of the peaks reported is the found from fitting the experimental curves by taking into account the two modes behavior (see text). The symbol * indicates that the corresponding mode could not be isolated in the respective Raman spectrum.

$x \longrightarrow$	0	0.66		1		1.5		2
	$\bar{\omega}$	$\bar{\omega}$-Nb	$\bar{\omega}$-V	$\bar{\omega}$-Nb	$\bar{\omega}$-V	$\bar{\omega}$Nb	$\bar{\omega}$-V	$\bar{\omega}$
$A_g(1)$	882	881	867	878	864	878	865	859
$B_{1g}(1)$	828	826	814	826	814	*	808	808
$B_{1g}(2)$	697	697	720	695	717	685	715	705
$A_g(3)$	530	534	562	541	575	549	571	579
$A_g(5)$	407	*	*	*	*	*	*	406
$B_{3g}(7)$	338	*	*	*	*	*	*	333
$A_g(7)$	298	*	*	*	*	*	*	293
$A_g(8)$	256	*	*	*	*	*	*	249
$A_g(9)$	224	*	*	*	*	*	*	220
$B_{1g}(11)$	174	*	*	*	*	*	*	173
$A_g(11)$	150	*	*	*	*	*	*	151
$A_g(12)$	82	74		75		77		81
$A_g(13)$	68	59		59		60		59

We will analyze the transformation of the Raman spectrum along the series $NiNb_{2-x}V_xO_6$ by dividing the spectrum in three different regions. The first region is above $\bar{\omega} = 800$ cm^{-1} where the most intense peak of each spectrum is observed; the relative wavenumber where the maximum of that peak appears varies from $\bar{\omega} = 882$ cm^{-1} for the sample $x = 0$ to $\bar{\omega} = 859$ cm^{-1} for the sample $x = 2$. The second region is between $\bar{\omega} = 500$ cm^{-1} and $\bar{\omega} = 800$ cm^{-1}; it presents very wide peaks in the samples with $0 < x < 2$. Finally, the third region is the one below $\bar{\omega} = 500$ cm^{-1} where the general aspect of the spectrum of the samples with $x > 0$ is similar. In this third region most of the modes are clearly identified only in the two extreme compounds; the modes of the sample $x = 0$ are observed at slightly higher or very close values of relative wavenumber compared to those in the sample $x = 2$.

In the higher wavenumber region the most intense peak of each spectrum is related to the B-O_t bonds and is observed at a value which is 22 cm^{-1} lower in the spectrum of NiV_2O_6 than in the spectrum of $NiNb_2O_6$. According to the Badger's rule, it can be considered that the relative wavenumber of the vibrational modes varies with the interatomic distance as $\bar{\omega} \propto 1/d^{3/2}$. Since the interatomic distance B-O_t is 13% less when B = V than when B = Nb (see third column of Table 4), the behavior observed in the spectra of our series of samples is opposite to that expected from the Badger's rule. A lack of the systematic expected from the simple dependence of $\bar{\omega}$ on the masses and interatomic distances was also observed in the Raman spectra of the several Niobates studied

Table 7: Structural environment of V^{+5}-cations in different compounds and relative wavenumber of the most intense peak in the region $\bar{\omega} > 700$ cm^{-1} ($\bar{\omega}_{A_{g'}}$). The acronyms are: SG ≡ Space group; CN ≡ coordination number in octahedral (Octa) or square pyramidal (Pyram) environment formed by the oxygen atoms; SS≡Site symmetry; RP ≡ room-pressure *The complete set of results for this compound will be published elsewhere.

Compound	SG	CN	SS	V-O$_t$ Å	P	$\bar{\omega}_{A_{g'}}$	Ref.
NiV_2O_6	*Pbcn*	6 - Octa	1	1.64	RP	859	
CoV_2O_6	*Pbcn*	6 - Octa	1	1.76	RP	852	*
MgV_2O_6	*Pbcn*	6 - Octa	1	1.69	RP	916	[12]
MgV_2O_6	*C2/m*	6 - Octa	m	1.67	4 GPa	910	[25]
MgV_2O_6	*C2*	6 - Octa	1	1.57	27 GPa	970	[25]
ZnV_2O_6	*Pbcn*	6 - Octa	1	1.66	RP	918	[26]
ZnV_2O_6	*C2/m*	6 - Octa	m	1.67	15 GPa	945	[27]
ZnV_2O_6	*C2*	6 - Octa	1	1.66	21 GPa	955	[27]
$\beta-V_2O_5$	*P21/m*	6 - Octa	m	1.58/1.65	RP	1021/942	[15, 28, 29]
$\alpha-V_2O_5$	*Pmmn*	5+1 - Piram	m	1.59	RP	996	[30, 29, 31]
La_2LiVO_6	*Fm3m*	6 - Octa		1.77	RP	730	[32, 33]

in Ref. [21]; there the anomalous variation of the relative wavenumber was explained by taking into account the electronegativity of the M^{+2} cations. In our case M = Ni^{+2} in both $x = 0$ and $x = 2$ samples; notwithstanding, the remaining idea is that physicochemical factors different from those considered in the simple form of the Badger's rule may have to be considered in order to explain the variation in relative wavenumber of the Raman modes from one compound to another. Below we will present some other examples of anomalous variations of the Raman relative wavenumber with the interatomic distance in different compounds even when the local environment of the ions remains similar.

Table 7 shows the position of the most intense peak in the region $\bar{\omega} > 700$ cm^{-1} of the Raman spectra in several compounds where the local environment of the V^{+5} cations is octahedral. Looking at the set of Vanadates AV_2O_6 (A = Ni, Co, Mg, Zn) with crystalline structure belonging to the *Pbcn* space group, one can see that the monotonic increase of the relative wavenumber with decreasing V-O$_t$ distance is not verified. As in Ref. [21], the higher electronegativity of nickel with respect to magnesium and zinc can explain the lower relative wavenumber of the A_g Raman mode involving the oxygen atoms in the terminal position even if the V-O$_t$ distance is smaller in the NiV_2O_6.

In both MgV_2O_6 [25] and ZnV_2O_6 [27] the room pressure structure (*C2/m*) decreases its symmetry presenting a phase transformation to a *C2*-phase when pressures of about 20 GPa and 17 GPa, respectively, are applied. The relative wavenumber of the most intense peak of the Raman spectrum of MgV_2O_6 ($\bar{\omega} = 922$ cm^{-1}) reduces when external pressure up to P = 3.9 GPa is applied, there an increasing in the coordination number (CN) from 5+1 to 6 occurs [25]. At higher

pressures the relative wavenumber of the Raman mode increases continuously until at least P = 28 GPa. In both the Mg and Zn cases the most intense peak of the Raman spectrum increases in relative wavenumber as the pressure increases. Simultaneous structural studies show that this shift in the Raman relative wavenumber is accompanied by an increasing distortion of the AO_6 and VO_6 octahedra. As can be seen in Table 7, in the case of MgV_2O_6 the reduction of symmetry between *C2/m* and *C2*-phases is accompanied by a decrease in the V-O distance and an increase in the relative wavenumber of the Raman mode. However, in the ZnV_2O_6 the CN, the octahedral environment and the V-O distance in the three structures (*Pbcn, C2/m* and *C2*) remains almost unaltered but the relative wavenumber of the Raman mode varies greatly and it is the highest for the less symmetric crystalline structure.

The case of V_2O_5 is interesting because the application of external pressure induces not only a phase transition to a crystalline phase of lower symmetry, but it also changes the local environment of the V^{+5} cation. The $\alpha-V_2O_5$, stable at room conditions, is formed by edge-sharing bi-pyramidal V_2O_4 chains where all the V-atoms have equivalent crystallographic positions [15, 31]. When pressures higher than P = 4.5 GPa are applied, an increasing of the CN from 5+1 to 6 accompanied of a structural phase transition from *Pmmn* to $P2_1/m$ space group is induced. In the high-pressure phase, β-V_2O_5, the crystallographic sites of V, O1, and O2 atoms split in two non equivalent positions which form two different octahedral environments for the V^{+5} cations [15, 31, 29, 28].In consequence, not one but two A_g peaks are observed in the Raman spectrum of the β-V_2O_5; one of those peaks is ascribed to one bond with interatomic V-O distance which is almost the same than that in the $\alpha-$phase (1.59 Å); however, an increase of 25 cm^{-1} is observed in the relative wavenumber of the mode of the $\beta-$phase with respect to the $\alpha-$one [29]. One can summarize these experimental observations by saying that the reduced symmetry of the overall structure and increasing CN favored an increasing in the relative wavenumber of the A_g mode in the β-V_2O_5 with respect to that of the α-V_2O_5.

If we compare now the *Pbcn*-NiV_2O_6 compound with the double perovskite La_2LiVO_6 where the octahedra are rather regular [32], a strong contrast appears. In the *Pbcn*-NiV_2O_6 the VO_6 octahedra are strongly distorted, so these two compounds can be taken as the extreme behavior of the V^{5+} state octahedral environment. In Table 7 it is clear that the La_2LiVO_6 shows by far the lowest relative wavenumber of the higher intensity peak, while the V-O distance is the same that in the *Pbcn*-CoV_2O_6. These facts, and those presented in the previous paragraphs point to a general conclusion in terms of the symmetry not only of the local environment but also of the overall crystalline structure where the V^{+5} ions are inserted. In general, the relative wavenumber of the highest intensity Raman peak is very sensitive to the specific details of the crystalline structure as a whole and so it behaves almost as a fingerprint of the compound; apparently this mode tends to appear at lower frequencies in more symmetric space groups and higher coordination numbers of the B-atoms.

Returning to the Raman spectra of the samples $NiNb_2O_6$ and NiV_2O_6 studied here, we will remind now some differences both in the local and global environments of the V^{+5} and Nb^{+5} cations. From the variation of the angles B-O-B, θ_1 and θ_2, and from the calculated dispersion of the B-O distances, we concluded that the VO_6 octahedra are more distorted than the NbO_6 ones.

The mean distance B-O is more than 7% less when B = V than when B = Nb, but it does not necessarily traduce in a higher stiffness of the B-O bonding. The lower B-O distance when B = V can be barely due to the fact that the effective radius of the V^{+5} ($r = 0.59$ Å) is smaller than the effective radius of Nb^{+5} ($r = 0.69$) [34]. In the counterpart, the higher effective nuclear charge of the Nb^{+5} ($Z_{\text{eff}} = 13.25$) with respect to that of the V^{+5} ($Z_{\text{eff}} = 11.8$) [33] could lead to higher force constants of the bonds even if the oxygen atoms are further in the former case. Additionally, we showed the previous paragraphs that the relative wavenumber of the most intense Raman peak is affected by the whole crystalline structure and not only by the local environment of the B-cations. If we look now to the nickel ions environment, the distortion calculated for the NiO_6 octahedra in the $x = 0$ sample is $\Delta = 6.89 \times 10^{-4}$, against $\Delta = 1.27 \times 10^{-4}$ in the $x = 2$ sample. Thus we conclude that, opposite to the situation of the B^{+5}-cations, the environment of the Ni^{+2}- cations is much more symmetric in the NiV_2O_6 than in the $NiNb_2O_6$. Then, it is a possibility that the force constant of the Ni-O bond is higher in the NiV_2O_6 than in the $NiNb_2O_6$ and that, similarly to the effect of the electronegativity, this weakens the force constant of the V-O bonds thus reducing the relative wavenumber of the most intense Raman peak with respect to that observed in the $NiNb_2O_6$ Raman spectrum.

Until now we have discussed mainly over the Raman spectra of the samples $x = 0$ and $x = 2$. We would like to focus now on the Raman spectra of the samples with intermediate quantities of niobium and vanadium, $0 < x < 2$. A common characteristic to all these samples is that their Raman spectra are mainly composed of very spread intensity distributions which correspond to obvious increasing from the background line, but where individual peaks can not be separated. It was said above that one part of the widening of the peaks seems to be intrinsic to the highly distorted VO_6 octahedra. However, the absence of a continuous evolution of the modes in the Raman spectrum with increasing vanadium content makes us think of a two-modes behavior as another contribution to the widening of the Raman peaks in the samples with both NbO_6 and VO_6 pseudo-octahedra.

The two modes evolution of the Raman spectra in a solid solution is well described in the study done for semiconductor alloys in Ref. [35]. Here, we can think of our samples of $NiNb_{2-x}V_xO_6$ as being formed by an increasing quantity of V-atoms getting forced into a $NiNb_2O_6$ matrix; the fact that the Raman spectrum evolves showing a two modes behavior along the series of samples means that the V-atoms do not spread homogeneously in the unitary cells of the matrix, and so one can not think of the existence of a virtual B-atom possessing intermediate properties between those of the niobium and those of the vanadium, but instead clusters of Nb and V-octahedra whose size evolves with the value of x along the solid solution. Due to the significant differences we saw in the NbO_6 and VO_6 structural blocks, the tendency towards clustering similar NbO_6 or else VO_6 octahedra is actually expected. In our samples, the widening of the Raman peaks due to cluster formations comes from the independent vibrations of the local bonds in the Nb and V-octahedra; these vibrations manifest separately thus making that the Raman peaks do not evolve so much in relative wavenumber but in intensity depending if the quantity of one determined atomic species increases or reduces. In general the clustering reduces the grain-size of each individual structure thus broadening the overall Raman signature. In fact, the segregation in clusters of the V-atoms in the very stable $NiNb_2O_6$ matrix is one possible explanation to why we observed some difficulty

to obtain the pure $x = 0.5$ sample. At this point it is worth to recall that Raman spectroscopy is a probe very sensitive to the local atomic environment, whereas the crystal structure analysis performed by XRD provides a complementary information averaging over several unit cells leading to mean interatomic distances. This averaging produces the sensation of having one single structural phase and a continuous evolution of the XRD pattern and the unit-cell parameters, but in the case of the samples with intermediate compositions of Nb and V it may not describe the real local atomic environment.

Because of the atomic vibrations in the NbO_6 and VO_6 octahedra manifest separately in the samples with intermediate composition of Nb and V, their experimental Raman spectra can be fitted by adding the separated contributions of peaks for the pure Nb and pure V samples. An illustration of how the two-modes behavior manifest in the most intense peak of the Raman spectra of our $NiNb_{2-x}V_xO_6$ series of samples is shown in Fig. 8. For the sample $x = 1$ it is exemplified in Fig. 8(a) that the form of the peak can be reproduced by joining the corresponding peaks to the Raman spectra of the samples with extreme compositions $x = 0$ and $x = 2$. The broadening that appears at the low wavenumber side is reproduced by the appearing of the peaks $B_g(1)$ (this is signaled by the symbol $\bullet$ in Fig. 7 for sample $x = 0$) and by taking into account an asymmetry of the peak $A_g(1)$ of sample $x = 2$. This asymmetry is possibly due to the same type of local disorder mentioned above to explain the widening of the Raman peaks of the NiV_2O_6 sample, and it is probably increased by the presence of octahedra with different sizes and in different exterior environments. The increasing of local disorder also manifests as a general enlargement of the FWHM of the individual peaks necessary to make the fitting of the Raman peaks of samples with intermediate compositions of Nb and V (see panel (c) of Fig. 8). The reduction of the contribution of the NbO_6 octahedra to the Raman spectrum as the V atoms are substituted for Nb ones is seen in the reduction of the ratio of the areas of individual peaks, A_{Nb}/A_V, with increasing x (Fig. 8(b)). Finally, the positions of the individual $A_g(1)$ peaks attributed to the Nb and V octahedra, which are used to fit the $A_g(1)$ peaks of the intermediate composition samples along the whole series, is plotted as a function of x in Fig. 8(d) and their values are presented in the third row of Table 6. The results of the fits performed in the region $500 < \bar{\omega} < 1000$ of the Raman spectra for all samples are shown in the supplementary material; the peaks that could be most clearly separated are also reported in columns 3 - 8 of Table 6.

We will consider now the second region of frequencies $(500 < \bar{\omega} < 800)$ cm^{-1} in the Raman spectra of our $NiNb_{2-x}V_xO_6$ series of samples. Disregarding the peak related to the mode B_{1g}, which is too wide or too weak to make any trustable analysis over it, the only peak remaining in this region is the one related to the mode $A_g(3)$ which describes the B-O_b stretching vibrations. Looking only at the two extreme compositions $x = 0$ and $x = 2$, the distances B-O_b are sensibly smaller when B = V than when B = Nb. Based on this statement, it is expected from the Badger's rule that the force constants of the V-O_b bonds are stronger than those of the Nb-O_b ones, and so the modes related to these bonds are expected to appear at higher frequencies in the NiV_2O_6 than in the $NiNb_2O_6$, as it is experimentally observed. Regarding now to the complete set of samples, one can track the monotonic increasing in the relative wavenumber where the maximum of the peak $A_g(3)$ is observed in Fig. 9; it varies from $\bar{\omega} = 530$ cm^{-1} for $x = 0$ to $\bar{\omega} = 580$ cm^{-1} for $x = 2$. However, as it can be verified in Table 4, the same monotonic behavior is not observed in any of the

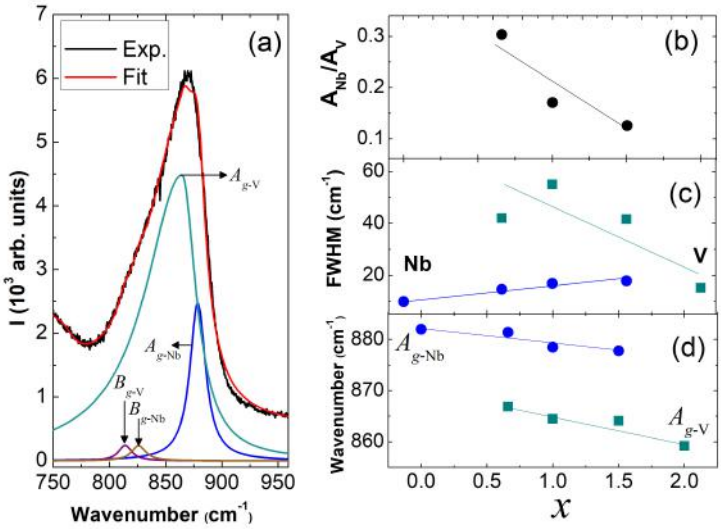

Figure 8: Two-modes behavior exemplified in the most intense peak $A_g(1)$ of the Raman spectra of the $NiNb_{2-x}V_xO_6$ series of samples. (a)Fitting of the highest Raman peak of sample $NiNbVO_6$, the fitting curve is the sum of peaks $A_g(1)$ and $B_g(1)$ of samples $x = 0$ and $x = 2$; (b)Ratio of the areas of peaks $A_g(1)$ for samples $x = 0$ (A_{Nb}) and $x = 2$ (A_V); (c)FWHM of the $A_g(1)$ peaks as a function of the vanadium content; (d)Variation in relative wavenumber of the peak $A_g(1)$ of Nb and V-octahedra with vanadium content. Solid lines are guides for the eyes

distances ascribed to the oxygen atoms in the bridge positions. In consequence, the linear behavior expected from the Badger's rule in the graphics $\bar{\omega}^2$ vs. $1/d^3_{\text{B-O}_b}$ is not verified (not shown). We should notice that in the frame of the two modes behavior, a possible reason for this is that the values calculated by the XRD represent mean B-O_b distances which may not correspond to a good representation of the real local environments of the Nb and V atoms. As it was discussed above, it is probable that because of the very different octahedral environments of the Nb and V atoms, the samples with $0 < x < 2$ are formed of clusters of separated VO_6 and NbO_6 octahedra which can not be represented by one virtual medium atom as the one considered by the XRD technique. Here we invoke again the two modes behavior in order to explain the evolution of the Raman peaks along our series of samples in this range of wavenumbers; it is exemplified for the mode $A_g(3)$ in the inset of Fig. 9 (a). Because of the contribution of neighbor peaks which are wider and closer in this region of the spectrum than in the higher relative wavenumbers, the fitting is more difficult and some shift in the center of the peaks attributed to the pure Nb and pure V-octahedra is even found as it can be seen in the panel (c) of Fig. 9 and in row six of Table 6.

In the third region of the spectra ($\bar{\omega} < 500$ cm $^{-1}$), following the different Raman modes across the solid solution is difficult because of a general broadening of the peaks in the samples with $x > 0$. The modes $A_g(12)$ and $A_g(13)$ which appear respectively at $\bar{\omega} = 82$ cm^{-1} and $\bar{\omega} = 68$ cm^{-1} in the spectrum of sample $x = 0$ show an abrupt shift to lower wavenumbers when x goes to 0.66. With further increasing proportion of V in the solid solution, the mode $A_g(12)$ increases

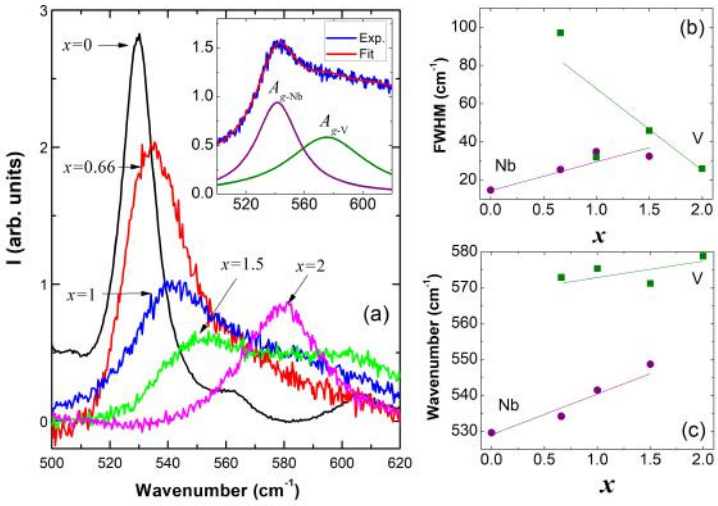

Figure 9: (a) Evolution of the Raman-mode $A_g(3)$ with the concentration of vanadium along the $NiNb_{2-x}V_xO_6$ series of samples; in order to improve the visualization, the data for $x = 0$ is multiplied by 0.5. The inset shows the experimental curve of the sample $x = 1$ fitted by the two-modes of the extreme compositions; (b)FWHM of the peaks used to perform the fitting of the $A_g(3)$ mode as a function of the vanadium content; (d)Variation in relative wavenumber of the center of the peaks just described along the whole series of samples. Solid lines are guides for the eyes

regularly in wavenumber to reach the same position in NiV_2O_6 as in $NiNb_2O_6$; whereas the mode $A_g(13)$ remains at a constant wavenumber of 60 cm^{-1} for all samples with $x \geq 0.66$. The modes $A_g(12)$ and $A_g(13)$ are controlled by the O-Nb-O/Ni-O-Nb bending and by the Ni-O stretching, respectively. The abrupt blue shift detected in the spectra of samples with $x > 0$ is in agreement with the increase of the Ni-O distances as deduced from the XRD results (see Table 3).

4 Conclusion

The compound NiV_2O_6 with the unusual columbite-type structure was successfully synthesized under conditions of high pressure and temperature. The structural characterization shows that this material is formed by two fundamental structural units of octahedral symmetry, one very regular around the Ni-atoms and one very distorted around the V-ones. While conserving the *Pbcn* structure, the gradual substitution of vanadium for niobium in the $NiNb_{2-x}V_xO_6$ series of compounds produces the anisotropic shrink of the unit-cell parameters: between the two extreme compositions the variation in the a and c parameters is almost the same but twice that observed in the b parameter. When compared, the BO_6 octahedral units of the NiB_2O_6-*Pbcn* compound are smaller but more distorted for B = V than for B = Nb; in contrast, the NiO_6 structural units are bigger and more symmetric in the former case.

We report the first Raman spectrum of the NiV_2O_6-*Pbcn* HPHT polymorph and extended the list of the previous observed modes for the $NiNb_2O_6$. The Raman spectrum of NiV_2O_6-*Pbcn* is characterized by relatively wide peaks. This widening was ascribed to the very distorted octahedron. The evolution of the Raman spectrum with increasing vanadium content along the series of samples $NiNb_{2-x}V_xO_6$ was analyzed by considering a two-modes behavior consisting in the formation of clusters of separated vanadium and niobium octahedra. The Raman spectra of the samples with intermediate compositions of Nb and V ($0 < x < 2$) are formed by a set of entangled peaks forming very broad structures all along the relative wavenumber ranges. These spectra contain the modes of vibration related to four different structural environments: NbO_6 octahedra, very distorted VO_6 octahedra and two NiO_6 octahedra with different sizes and distortion indexes. The enlargement of the Raman peaks of the samples with intermediate compositions of Nb and V shows that there is an inhomogeneous distribution of Nb and V-octahedra leading to structural disorder and atomic segregation. The comparison of the higher wavenumbers region of the Raman spectra of $NiNb_2O_6$ and NiV_2O_6 led us to conclude that the smaller size of V^{+5}, which favors an increasing symmetry of the structural arrangement of oxygen around the central Ni atom, boosts the ionic character of the Ni-O bonds in the samples rich in vanadium. This however contributes to reduce the force constant of the V-O bonds inside the VO_6 octahedra letting it even lower than that in the NbO_6 octahedra despite of the lower V-O distances. This can imply very important differences in the physical properties of these two compounds.

Further theoretical studies may be necessaries in order to completely understand the observed changes in the Raman spectrum along the series of samples $NiNb_{2-x}V_xO_6$ studied here.

5 Aknowledgments

This work was financed by the french-brazilian cooperation program 'CAPES-COFECUB', process 88887.321681/2019-00, and the french institution 'Centre National de la Recherche Scientifique', CNRS. We thank to the professional team of the X-Press pole of the 'Néel Institut', specially Celine Goujon and Murielle Legendre for the technical support in the preparation of the samples.

References

[1] T. Hanawa, K. Shinkawa, M. Ishikawa, K. Miyatani, K. Saito, and K. Kohn, "Anisotropic Specific Heat of $CoNb_2O_6$ in Magnetic Fields," *Journal of the Physical Society of Japan*, vol. 63, p. 2706, July 1994.

[2] C. Heid, H. Weitzel, F. Bourdarot, R. Calemczuk, T. Vogt, and H. Fuess, "Magnetism in $FeNb_2O_6$ and $NiNb_2O_6$," *Journal of Physics Condensed Matter*, vol. 8, pp. 10609–10625, Dec. 1996.

[3] P. W. C. Sarvezuk, M. A. Gusmão, J. B. M. da Cunha, and O. Isnard, "Magnetic behavior of the $Ni_xFe_{1-x}Nb_2O_6$ quasi-one-dimensional system: Isolation of Ising chains by frustration," *Phys. Rev. B*, vol. 86, p. 054435, Aug. 2012.

[4] J. Ye, Z. Zou, and A. Matsushita, "A novel series of water splitting photocatalysts NiM_2O_6(M = Nb, Ta) active under visible light," *International Journal of Hydrogen Energy*, vol. 28, no. 6, pp. 651 – 655, 2003. CANCUN-01.

[5] M. L. Hneda, J. B. M. da Cunha, A. Popa, and O. Isnard, "Magnetic order suppression and structural characterization of $MnNb_{2-x}V_xO_6$ columbites crystallized under extreme pressure conditions," *Journal of Magnetism and Magnetic Materials*, vol. 496, p. 165907, Feb. 2020.

[6] E. J. Baran, C. I. Cabello, and A. G. Nord, "Raman spectra of some $MIIV_2O_6$ brannerite-type metavanadates," *Journal of Raman Spectroscopy*, vol. 18, pp. 405–407, Sept. 1987.

[7] M. Markkula, A. M. Arevalo-Lopez, and J. Paul Attfield, "Neutron diffraction study of monoclinic brannerite-type CoV_2O_6," *Journal of Solid State Chemistry France*, vol. 192, pp. 390–393, Aug. 2012.

[8] M. Lenertz, J. Alaria, D. Stoeffler, S. Colis, A. Dinia, O. Mentré, G. André, F. Porcher, and E. Suard, "Magnetic structure of ground and field-induced ordered states of low-dimensional α-CoV_2O_6: Experiment and theory," *Phys. Rev. B*, vol. 86, p. 214428, Dec. 2012.

[9] Driele, Von Dreifus and Rodrigo, Pereira and Ariano, D. Rodrigues and Ernesto, C. Pereira and Adilson, J.A. de Oliveira, "Sol-gel synthesis of triclinic cov2o6 polycrystals," *Ceramics International*, vol. 44, no. 16, pp. 19397 – 19401, 2018.

[10] M. Gondrand, A. Collomb, J. C. Joubert, and R. D. Shannon, "Synthesis of new high-pressure columbite phases containing pentavalent vanadium," *Journal of Solid State Chemistry France*, vol. 11, pp. 1–9, Sept. 1974.

[11] M. L. Hneda, J. B. M. da Cunha, M. A. Gusmão, S. R. O. Neto, J. Rodríguez-Carvajal, and O. Isnard, "Low-dimensional magnetic properties of orthorhombic MnV_2O_6 : A nonstandard structure stabilized at high pressure," *Phys. Rev. B*, vol. 95, p. 024419, Jan. 2017.

[12] R. L. Tang, Y. Li, Q. Tao, N.-N. Li, H. Li, D. D. Han, P. W. Zhu, and X. Wang, "High-pressure Raman study of MgV_2O_6 synthesized at high pressure and high temperature," *Chinese Physics B*, vol. 22, p. 066202, June 2013.

[13] M. Belaiche, M. Bakhache, M. Drillon, A. Derrory, and S. Vilminot, "Magnetic properties of MV_2O_6 compounds (M = Cu, Co, Ni)," *Physica B Condensed Matter*, vol. 305, pp. 270–273, Nov. 2001.

[14] H. X. Dang, A. J. E. Rettie, and C. B. Mullins, "Visible-light-active niv_2o_6 films for photoelectrochemical water oxidation," *The Journal of Physical Chemistry C*, vol. 119, no. 26, pp. 14524–14531, 2015.

[15] P. Shvets, O. Dikaya, K. Maksimova, and A. Goikhman, "A review of Raman spectroscopy of vanadium oxides," *Journal of Raman Spectroscopy*, vol. 50, pp. 1226–1244, Aug. 2019.

[16] J. Rodríguez-Carvajal, "Recent advances in magnetic structure determination by neutron powder diffraction," *Physica B Condensed Matter*, vol. 192, pp. 55–69, Oct. 1993.

[17] K. Momma and F. Izumi, "*VESTA3* for three-dimensional visualization of crystal, volumetric and morphology data," *Journal of Applied Crystallography*, vol. 44, pp. 1272–1276, Dec 2011.

[18] M. Wojdyr, "*Fityk*: a general-purpose peak fitting program," *Journal of Applied Crystallography*, vol. 43, pp. 1126–1128, Oct 2010.

[19] E. Husson, Y. Repelin, N. Q. Dao, and H. Brusset, "Normal coordinate analysis for $CaNb_2O_6$ of columbite structure," *J. Chem. Phys.*, vol. 66, pp. 5173–5180, June 1977.

[20] E. Husson, Y. Repelin, N. Q. Dao, H. Brusset, and E. Fardouet, "Etude par spectrophotométries d'absorption infrarouge et de diffusion Raman des niobates de structure columbite," *Spectrochimica Acta Part A: Molecular Spectroscopy*, vol. 33, pp. 995–1001, Jan. 1977.

[21] E. Husson, Y. Repelin, N. Q. Dao, and H. Brusset, "Normal coordinate analysis of the MNb_2O_6 series of columbite structure (M=Mg, Ca, Mn, Fe, Co, Ni, Cu, Zn, Cd)," *J. Chem. Phys.*, vol. 67, pp. 1157–1163, Aug. 1977.

[22] I. D. Brown and R. D. Shannon, "Empirical bond-strength–bond-length curves for oxides," *Acta Crystallographica Section A*, vol. 29, no. 3, pp. 266–282, 1973.

[23] F. Huang, Q. Zhou, L. Li, X. Huang, D. Xu, F. Li, and T. Cui, "Structural Transition of $MnNb_2O_6$ under Quasi-Hydrostatic Pressure," *The Journal of Physical Chemistry C*, vol. 118, no. 33, pp. 19280–19286, 2014.

[24] E. Husson, Y. Repelin, N. Q. Dao, and H. Brusset, "Normal coordinate analysis for $CaNb_2O_6$ of columbite structure," *J. Chem. Phys.*, vol. 66, pp. 5173–5180, June 1977.

[25] R. Tang, Y. Li, S. Xie, N. Li, J. Chen, C. Gao, P. Zhu, and X. Wang, "Exploring the coordination change of vanadium and structure transformation of metavanadate MgV_2O_6 under high pressure," *Scientific Reports*, vol. 6, p. 38566, Dec. 2016.

[26] A. Beltrán, L. Gracia, and J. Andrés, "Polymorphs of ZnV_2O_6 under Pressure: A First-Principle Investigation," *The Journal of Physical Chemistry C*, vol. 123, no. 5, pp. 3239–3253, 2019.

[27] R. Tang, Y. Li, D. Han, H. Li, Y. Zhao, C. Gao, P. Zhu, and X. Wang, "A Reversible Structural Phase Transition in ZnV_2O_6 at High Pressures," *The Journal of Physical Chemistry C*, vol. 118, 5 2014.

[28] A. Grzechnik, "Local Structures in High Pressure Phases of V_2O_5," *Chemistry of Materials*, vol. 10, no. 9, pp. 2505–2509, 1998.

[29] R. Baddour-Hadjean, M. B. Smirnov, K. S. Smirnov, V. Y. Kazimirov, J. M. Gallardo-Amores, U. Amador, M. E. Arroyo-de Dompablo, and J. P. Pereira-Ramos, "Lattice Dynamics of $\beta-V_2O_5$: Raman Spectroscopic Insight into the Atomistic Structure of a High-Pressure Vanadium Pentoxide Polymorph," *Inorganic Chemistry*, vol. 51, no. 5, pp. 3194–3201, 2012. PMID: 22360539.

[30] B. Zhou and D. He, "Raman spectrum of vanadium pentoxide from density-functional perturbation theory," *Journal of Raman Spectroscopy*, vol. 39, pp. 1475–1481, Oct. 2008.

[31] L. Abello, E. Husson, Y. Repelin, and G. Lucazeau, "Vibrational spectra and valence force field of crystalline V_2O_5," *Spectrochimica Acta Part A: Molecular Spectroscopy*, vol. 39, pp. 641–651, Jan. 1983.

[32] J.-H. Choy, S.-H. Byeon, and G. Demazeau, "IR, Raman, and X-ray photoelectron spectroscopy investigations of the ordered cubic perovskite La_2LiVO_6," *Journal of Solid State Chemistry France*, vol. 76, pp. 97–101, Sept. 1988.

[33] G. Demazeau, E. Oh-Kim, J. Choy, and P. Hagenmuller, "A vanadate (V) oxide with perovskite structure: comparison with homologous La_2LiMO_6 phases (M = Fe, Nb, Mo, Ru, Ta, Re, Os, Ir)," *Materials Research Bulletin*, vol. 22, no. 6, pp. 735 – 740, 1987.

[34] R. Shannon and C. Prewitt, "Effective ionic radii in oxides and Fluorides," *Acta Cryst.*, vol. 25, p. 925, May 1968.

[35] O. Pagès, A. V. Postnikov, M. Kassem, A. Chafi, A. Nassour, and S. Doyen, "Unification of the phonon mode behavior in semiconductor alloys: Theory and ab initio calculations," *Phys. Rev. B*, vol. 77, p. 125208, Mar. 2008.